ChemComm

HIGHLIGHT

Check for updates

Dynamic evolution of metal–nitrogen–codoped carbon catalysts in electrocatalytic reactions

Zixuan Han, Yanmei Shi, [iD] Bin Zhang [iD] * and Lingjun Kong [iD] *

Atomic metal–nitrogen–codoped carbon (M–N–C) catalysts are highly efficient for various electrocatalytic reactions because of their high atomic utilization efficiency. However, the high surface energy of M–N–C catalysts often results in stability issues in electrochemical reactions. Therefore, understanding the stability and dynamic evolution of M–N–C catalysts is crucial for elucidating the active centers and the composition/structure–activity relationship. This review summarizes the factors affecting the durability of atomic catalysts in electrochemical reactions and discusses possible changes in catalysts during these electrochemical processes. Finally, advanced characterization techniques are described, with a focus on tracking the dynamic evolution of M–N–C catalysts during electrocatalysis. This review offers insights into the rational optimization of M–N–C electrocatalysts and provides a framework for linking their composition and structure with their catalytic activity in future research.

1. Introduction

Given the increased energy demands and environmental challenges, there is a growing need to transition from traditional fossil fuels to clean energy sources. Recent advancements in energy conversion technologies, such as water splitting, metal–air batteries, and fuel cells, have made significant strides toward achieving "carbon-free" energy conversion between electrical and chemical forms. The key electrochemical reactions involved in these technologies include the oxygen reduction reaction (ORR),[1] carbon dioxide reduction reaction (CO_2RR),[2] hydrogen evolution/oxygen evolution reaction (HER/OER),[3,4] and nitrogen oxyanion reduction reaction,[5,6] which typically involve multielectron transfer processes.[7] Therefore, efficient electrocatalysts are crucial for accelerating these electrochemical processes and reducing energy costs, thereby contributing to the transition toward cleaner energy and environmental sustainability.[1]

Recent research has focused extensively on atomic metal–nitrogen–codoped carbon (M–N–C) materials, which have garnered attention in the fields of energy and catalysis.[8–12] Like traditional porphyrin and phthalocyanine derivatives, M–N–C materials featuring specific metal centers and flexible structures are considered highly promising for electrochemical applications.[13,14] Functional groups such as pyridine-N, pyrrole-N, and graphite-N provide ample coordination sites, thereby anchoring metal atoms and preventing their aggregation into particles. This leads to M–N–C catalysts with maximized metal

atom utilization and unique geometric electronic structures, thereby offering catalytic activities comparable to those of precious metal-based catalysts.[10,15] Furthermore, N-doped carbon-based substrates exhibit advantageous properties, including large surface areas, excellent electrochemical performance, and high-density anchoring sites for metal atoms.[16] Additional functional groups containing oxygen, sulfur, and carbon can also serve as anchoring sites on the carbon matrix,[17–21] influencing charge distribution and tailoring active sites at the atomic level, thereby overcoming limitations in single-site-induced scaling relationships.

Significant efforts have been devoted to designing and developing M–N–C electrocatalysts to enhance electrocatalytic performance.[22] Controllable fabrication of these M–N–C catalysts with different compositions and morphologies is a common strategy to optimize their reactivity and increase the number and density of active sites.[23–25] However, during electrochemical reactions, the morphology and coordination structure of M–N–C catalysts can change, thereby leading to discrepancies between the as-synthesized structure and real active structures. High surface energy can make these catalysts susceptible to dissolution or transformation under specific conditions,[26,27] which can complicate the understanding of their catalytic mechanisms and structure–activity relationships. Furthermore, investigating the mechanisms behind dynamic restructuring is essential for a comprehensive understanding of these reactions. Therefore, any assessment of the structure–activity relationship of M–N–C catalysts must be accompanied by a parallel study of their structural dynamic behavior.[28–31]

This review aims to provide a comprehensive overview of the dynamic evolution of M–N–C catalysts during electrochemical

Institute of Molecular Plus, Department of Chemistry, School of Science, Tianjin University, Tianjin 300072, China. E-mail: bzhang@tju.edu.cn, ljkong@tju.edu.cn

reactions, which is an increasingly important topic. These factors affect the stability of M–N–C catalysts in electrochemical reactions, including internal factors (metal centers and coordination configurations) and external stimuli (pH and applied voltage). The dynamic behaviors of M–N–C catalysts, including reversible and irreversible structural changes during electrochemical processes, are systematically reviewed. Advanced characterization techniques for revealing structural changes and *in situ* dynamic evolution are also discussed. Finally, this review offers conclusions and a comprehensive outlook on future directions for M–N–C catalysts. This review is expected to guide the rational design of more efficient active sites in catalysts and the modulation of their dynamic evolution.

2. Factors affecting the stability of M–N–C catalysts

To evaluate the stability of an M–N–C catalyst, it is crucial to assess whether the chemical bonds forming the substance possess sufficient strength, as this is the fundamental reason behind variations in stability. Notably, M–N–C catalysts exhibit diverse structures, with variations in metal centers, coordination bonding energies, and configurations. On the basis of crystal field theory,[32] factors such as the geometric configuration, oxidation state, and period of the central metal atom, as well as the ligand field strength, significantly influence the primary stability of M–N–C catalysts. In electrocatalytic processes, the M–N–C catalysts interact with electrolytes; thus, nonelectrochemical effects from electrolyte conditions, especially pH, are a significant factor affecting their stability. Additionally, when a voltage is applied, the active centers in M–N–C catalysts can be further affected. The adsorption and desorption of reactants, intermediates, and products during the electrocatalytic process also affect the structure of M–N–C catalysts.[33] Current research highlights that both inherent factors (metal centers and coordination configurations) and external factors (solvents, pH, applied voltage, and adsorption dynamics) affect the stability of M–N–C catalysts in electrochemical reactions.[34,35] An overview of these factors on M–N–C stability is shown in Fig. 1.

2.1. Inherent factors

Structural features, including metal centers and coordination configurations, are critical inherent factors affecting the stability of M–N–C materials. The observed stability variations were attributable to differences in the bonding energies of the metal sites interacting with the intermediates. For example, Wu *et al.* reported that the Mn–N–C catalyst exhibited significantly enhanced stability in acidic media compared with the traditional Fe–N–C catalyst, as indicated by steady-state ORR polarization plots.[36] It was observed that the Fe–N–C and Co–N–C catalysts were prone to oxidative degradation because of the generation of reactive oxygen species such as hydroxyl radicals *via* Fenton reactions involving H_2O_2, an inevitable intermediate generated during the ORR process. Conversely, Mn–N–C
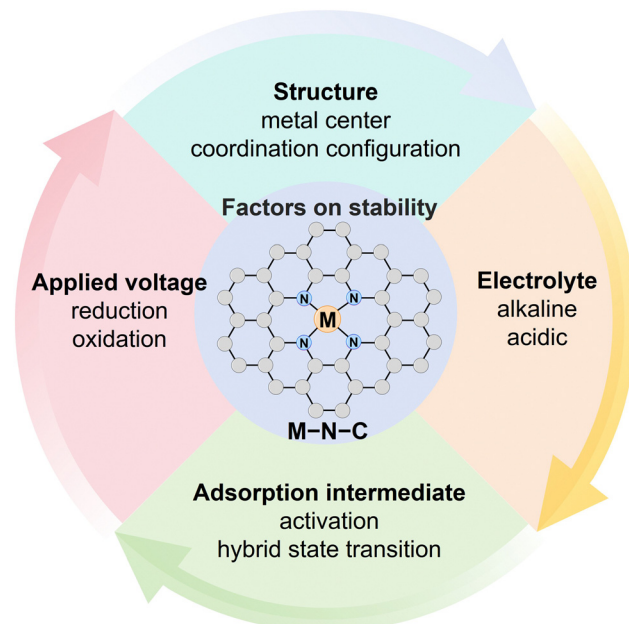

Fig. 1 Factors on the stability of M–N–C catalysts.

exhibited higher stability due to its relatively low catalytic activity for the Fenton reaction. He *et al.* also reported that Mn centers exhibited minimal reactivity with H_2O_2 compared with those with Fe and Co, thereby indicating higher stability in the ORR process.[37]

Coordination configurations, such as the coordination number and coordination atom type, also play a significant role in the stability of M–N–C catalysts.[38–42] The synthesis of M–N–C materials typically involves high-temperature calcination or acid etching, which often introduces carbon defects and dangling bonds on the catalyst surface. Studies have shown that the stability of M–N–C is highly sensitive to local coordination due to the unsaturated coordination environment of their support. The presence of atoms near the metal sites can significantly impact their electronic properties and local structure.[18,43] Even under long-term exposure to air, oxygen, and light can further react with these highly active species.[44] Coordination configurations are therefore recognized as key factors in regulating bond strength and electronic structure, thereby affecting M–N–C stability.[45] Jaouen *et al.* prepared an Fe–N–C catalyst with two distinct FeN_x sites (S1 and S2) *via* Mössbauer spectroscopy (Fig. 2).[46] Furthermore, the S1 site irreversibly transformed into an iron oxide (Fe_2O_3) under operating conditions during ORR catalysis, whereas the S2 site remained stable. Structure–activity correlations from the end-of-test ^{57}Fe Mössbauer spectroscopy revealed that both sites initially contribute to the ORR activity of Fe–N–C in an acidic medium. Only the S2 site substantially contributed after 50 h of operation. Li *et al.* developed P(AA-MA)–Fe–N and PAA–Fe–N ORR electrocatalysts with different Fe–N bond lengths and coordination. P(AA-MA)–Fe–N, with $Fe-N_4/C$ moieties and longer Fe–N, exhibited exceptional stability compared with that of PAA–Fe–N, which exhibited approximately 15% low-coordinated $Fe-N_2/N_3$ structures.[40]
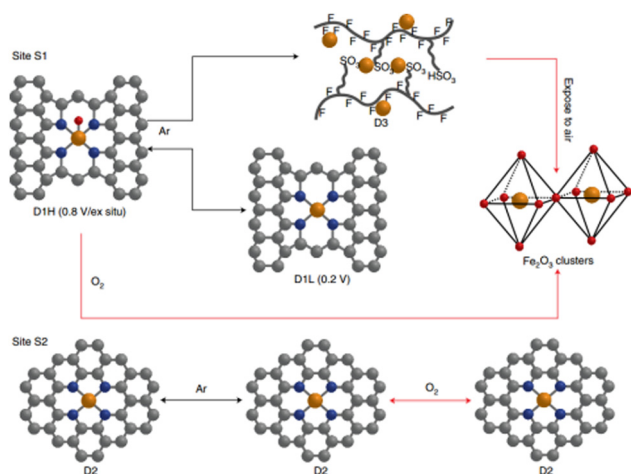
Fig. 2 Coordination or structural changes of the sites S1 and S2 under *operando* conditions in the electrochemical ORR process.[46] Copyright 2021, Springer Nature.

Fig. 3 (a) Schematic representation of ORR properties stability oxidation state in FeMn−N−C and the half-wave potential degradation of FeMn−N−C and Fe−N−C after CV cycles.[51] Copyright 2024, Wiley-VCH. (b) The formation energy heatmap for the M−N−C. (c) The structure of the di-carbon atom vacancy site and the two quad-atom carbon vacancy sites (QV2 and QV3).[52] Copyright 2023, Wiley-VCH.

Recent studies have shown that introducing a second metal atom component into the single transition metal M−N−C can increase stability by altering the geometry of the active site and the surrounding chemical environment.[47–50] Peng *et al.* constructed a FeMn−N−C dual-atom catalyst. Specifically, they quantitatively compared the Fe−N bond strengths in FeMn−N−C and Fe−N−C catalysts *via* crystal orbital Hamilton population (COHP) analysis. The integrated COHP (–ICOHP) value of the Fe−N bond increased from 1.264 to 1.971 upon the introduction of Mn, indicating that additional free electrons increased the electron density around Fe−N_4. This lowered the oxidation state of Fe, strengthened the Fe−N bond, and effectively inhibited the electrochemical dissolution of Fe.[51] Subsequently, the increased electrochemical stability of FeMn−N−C was confirmed through linear sweep voltammetry (LSV) conducted after 10 000, 20 000, and 50 000 cycles of CV (Fig. 3a). Karmodak *et al.* used formation-energy calculations and microkinetic modelling to demonstrate that increasing the number of metal dopants can effectively tune both the catalytic activity and stability of M−N−C (Fig. 3b and 3c).[52] Metal–metal interactions in the M−N−C structure reduce the dissolution of metal dopants under various electrochemical conditions. For M−N−C catalysts, four possible candidates, MnMn, FeFe, CoCo, and MnNi doped on quad-atom vacancy sites, have shown considerable stability across a wide pH range.

2.2. External factors

2.2.1. pH. Electrolytes (primarily acid–alkaline) are significant external factors affecting the stability and activity of M−N−C catalysts in electrocatalytic reactions.[53] Theoretical and experimental studies have shown that M−N−C catalysts exhibit insufficient stability under relevant pH conditions, thereby undergoing rapid degradation under acidic conditions.[54] For example, in an acidic ORR process, some isolated traditional metal atoms can easily dissolve during the catalytic process, thereby resulting in insufficient stability. Among the various
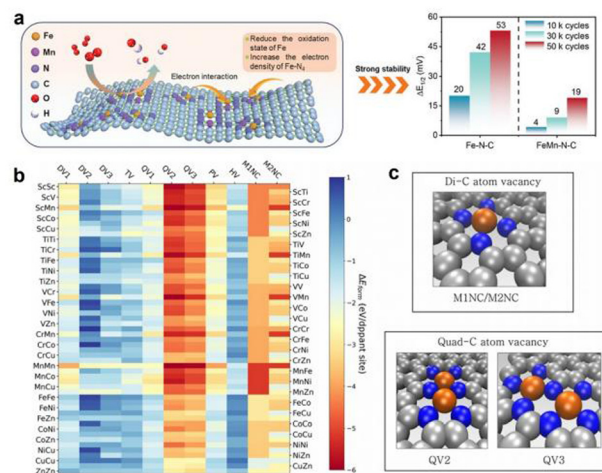
degradation mechanisms, protonation of the surrounding coordinated N atoms is generally attributed to the dissolution of metal centers in acidic media.[52] Furthermore, dissolution is more challenging under acidic conditions than under alkaline conditions, as reported in previous studies.[55,56] In alkaline media, some species, such as *OH, may attach to the surface of the metal site to enhance stability. Hansen *et al.* reported that a single Fe metal atom was susceptible to leaching from an Fe−N−C system with various considered structures (FeN_4C_{10}, FeN_4C_{12}, FeN_4C_A, and FeN_4C_Z) and FeN_3C_{10} under acidic ORR-related conditions.[43] Under a similar potential range under alkaline conditions, *OH and *O were formed from water at the Fe metal site on these structures, thereby stabilizing the Fe metal site against dissolution. However, the FeN_4C_8, FeN_3C_Z, and FeN_3C_A structures were susceptible to dissolution even under alkaline conditions, and the most stable phase was still a dissolved Fe compound. Wang and coworkers employed electrochemical tests and impregnation experiments to determine the stability of the synthesized Ni−N−C catalyst.[54] The initial stable Ni−N structure in Ni−N−C exhibited unconventional reconstruction under the OER to form Ni−O coordination. This was not only stable in real reactive centers under alkaline conditions during OER catalysis but also unstable under acidic conditions (Fig. 4a). Furthermore, increasing the chronoamperometry test time led to more severe metal leaching after acid impregnation, thereby indicating the continuous structural evolution process (Fig. 4b). Furthermore, Fe−N−C, Co−N−C, and Cu−N−C catalysts were synthesized and tested to determine the universality of this structural evolution process (Fig. 4c).

2.2.2. Applied voltage. The applied voltage is another significant external factor for the stability of M−N−C catalysts. Given the difference in the potential ranges of electrocatalytic reactions, the possible effects on M−N−C catalysts vary when
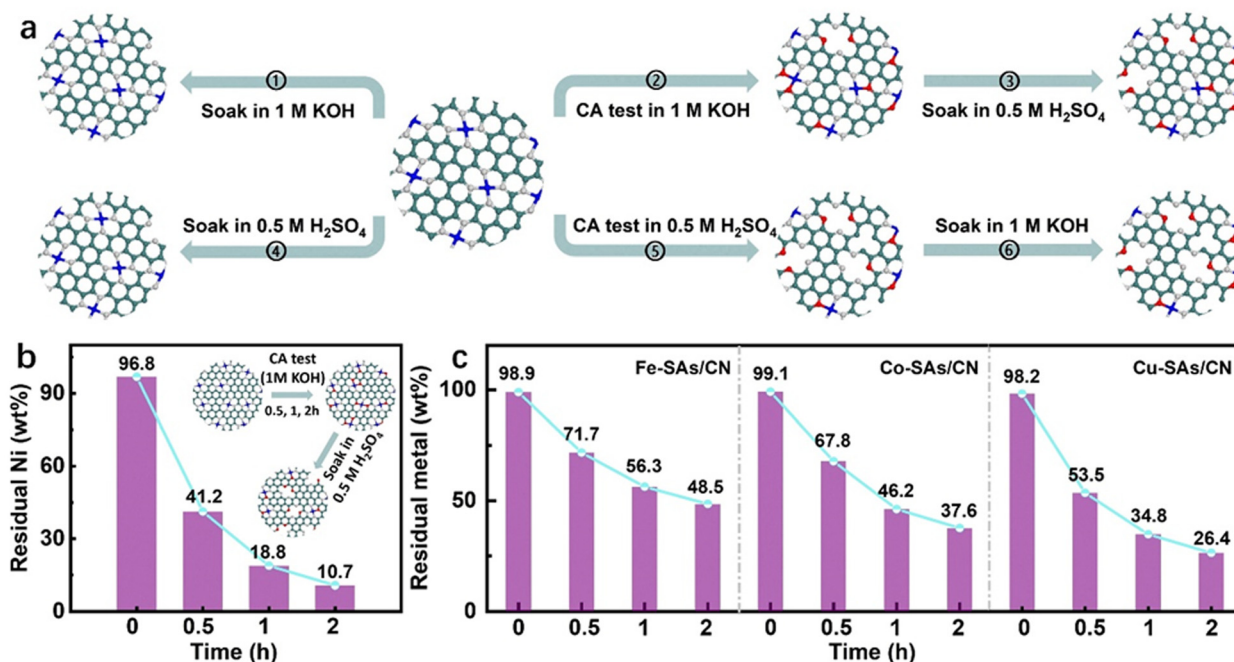
Fig. 4 (a) The solution impregnation and electrochemical OER test procedures on the Ni–N–C catalyst (b) Ni–N–C and (c) Fe–N–C, Co–N–C and Cu–N–C catalysts after chronoamperometry test in 1.0 M KOH at 1.53 V *vs.* RHE for different times with acid solution immersing treatment afterward.[54] Copyright 2024, Wiley-VCH.

the applied voltage is in the high-oxidative region. Specifically, in the OER, the metal centers of M–N–C catalysts are irreversibly oxidized to high valences or dissolve owing to the unstable coordination bonds formed by the metal center and non metal ligands.[57] Researchers have employed energy differences as indicators to evaluate the preferred redox behavior, metal center redox, and oxygen redox.[58] For example, Wang *et al.* observed a typical Ni–N–C material.[54] The results indicated that the theoretical Fermi energy of the Ni–N–C catalyst was −4.26 eV, which exceeded the thermodynamic oxidation potential of water (−4.84 eV). Thus, Ni–N–C underwent electron drain and subsequent oxidation processes.[58] Furthermore, when the applied voltage was in the reduction region (ORR, HER, and NO_3^-RR), the overnegative potentials led to the reduction of M–N–C catalysts. In another study, Wang *et al.* synthesized $Cu-N_4-C$ materials as nitrate reduction reaction (NO_3^-RR) catalysts and investigated their structural changes during the nitrate-to-ammonia electrocution process.[59] The reduction of Cu^{2+} to Cu^+ and Cu^0 as well as the subsequent aggregation of single Cu atoms facilitated the switching of the applied voltage from 0.0 to −1.0 V *vs.* RHE in the alkaline electrolyte (Fig. 5). *Operando* X-ray absorption spectroscopy (XAS) revealed successive structural transformations from $Cu-N_4$ to $Cu-N_4$/Cu-nanoclusters and subsequently to $Cu-N_3$/Cu-nanoclusters during the ORR process.

Stability diagrams of the M–N–C catalysts facilitated the thermodynamic understanding of their dissolution in aqueous media.[60] They are usually constructed through density functional theory (DFT)-based thermodynamic analysis on the basis of the well-known formalism of Pourbaix diagrams. Therefore,
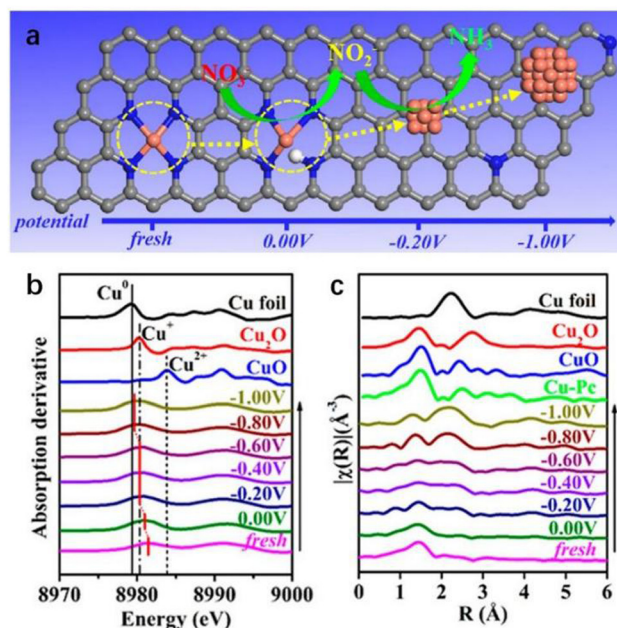

Fig. 5 (a) Potential-driven structural evolution of Cu–N–C in nitrate reduction. (b) First-order derivatives of the XANES spectra at different cathodic potentials. (c) Corresponding Cu K edge FT-EXAFS spectra at different potentials.[59] Copyright 2022, American Chemical Society.

the stability diagrams are called Pourbaix diagrams. Upon extending these approaches to proposed M–N–C active site structures, the stability dependence on pH and applied voltage was explored, thereby providing direct theoretical evidence.[61]
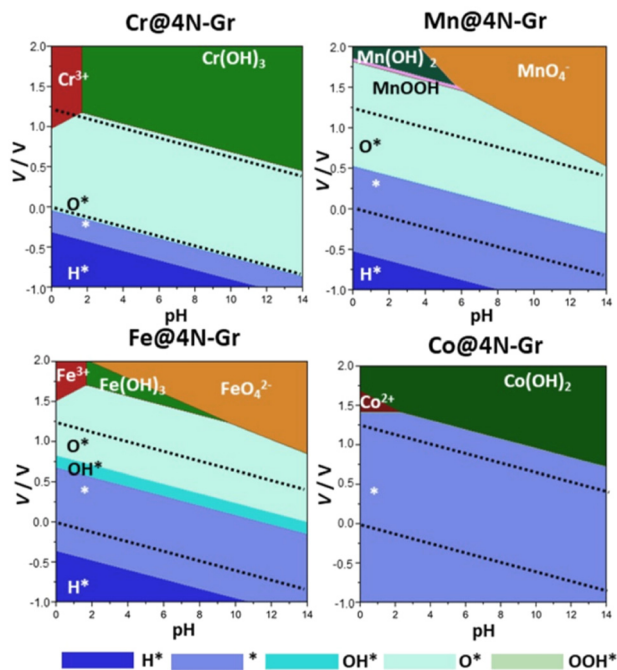
Fig. 6 Pourbaix diagrams of Cr@4N-Gr, Mn@4N-Gr, Fe@4N-Gr, and Co@4N-Gr[26] Copyright 2024, American Chemical Society.

Fig. 7 (a) Radical elimination rate statistics by using the ABTS radical concentration in Fe-NC$_{Phen}$ catalyst as the standard. (b) EPR spectra analysis of the *OH elimination by Fe-NC$_{Phen}$, Fe-NC/Sca^{CeO2}, and Fe-NC/Sca$^{ad-CeO2}$ (c) ORR polarization curves before and after 10 000 potential cycles in O$_2$-purged 0.1 M H$_2$SO$_4$ of Fe-NC$_{Phen}$, Fe-NC/Sca^{CeO2} and Fe-NC/Sca$^{ad-CeO2}$.[68] Copyright 2023, Wiley-VCH.

Thus, stability diagrams have been regarded as simple but effective forecasting approaches for estimating the relative stability of M–N–C catalysts. The redox potential of M–N–C catalysts was derived because different phases of the oxidation and reduction states of the materials exist under the given electrochemical conditions of pH and applied voltage. Examples of stability diagram construction for M–N–C can be found in recent reports.[60] Pacchioni *et al.* predicted the stability of different atoms supported on 4N-doped graphene (4N-Gr) *via* stability diagrams (part of the information was drawn from experiments and the others from DFT calculations).[26] As shown in Fig. 6, Cr@4N-Gr tended to dissolve under rather strong oxidative conditions. Under acidic conditions, Cr^{3+} complexes can even form Cr(OH)$_3$. Co@4N-Gr was stable in its clean state under both reducing and oxidative conditions, whereas Mn@4N-Gr and Fe@4N-Gr were covered by adsorbed species. All the M–N–C materials were dissolved and precipitated at high oxidative potentials depending on the working conditions. Other important variables, such as temperature, additive ions, and the adsorption of reaction intermediates, are rarely shown on the ideal stability diagram of M–N–C materials.[62,63] For this reason, additional research is needed on the stability diagram of M–N–C materials to effectively represent real situations.

2.2.3. Adsorbed substances. Electrochemical reactions are further complicated by the fact that, in addition to external factors such as pH and applied voltage, the adsorption of reactants, intermediates, or products can significantly affect the stability of metal sites in the M–N–C structure.[33,64] Pasti *et al.* conducted a thermodynamic analysis of M–N–C with various metal atoms embedded into the N$_4$ moiety in graphene *via* DFT. The metal centers were covered with H, O, and OH
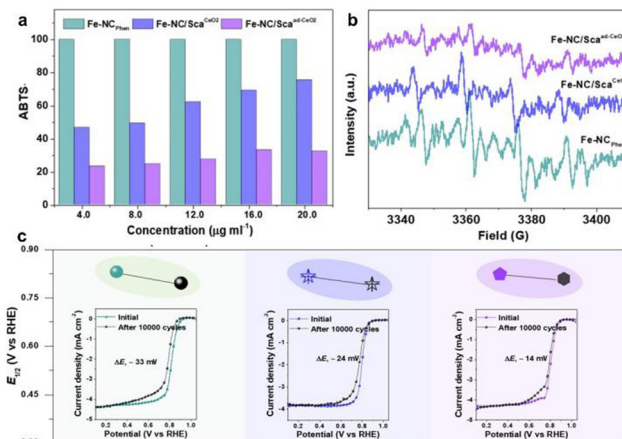
groups at any potential or pH within the water thermodynamic stability region, thereby leading to blockage and restructuring of the metal active sites.[65] For example, in the ORR process, O$_2$-accessible M–N$_x$ sites are attacked by radicals, such as •OH and HO$_2$•, which are considered among the most critical sources of M–N–C degradation.[36] Additionally, H$_2$O$_2$-derived radicals induce carbon oxidation during the ORR process, which leads to various oxygen functional groups on the carbon surface. These groups deactivate the metal site and trigger irreversible leaching of the metal site.[46,66] Carbon corrosion also occurs, thereby leading to carbon loss surrounding the metal site and ultimately resulting in the reduced durability of high-performance ORR catalysts.[67] To mitigate the degradation mechanism of M–N–C catalysts, several strategies have been proposed, such as the introduction of a cocatalyst and free radical scavenger at the active sites. Sun *et al.* developed an innovative approach to effectively eliminate radicals by anchoring CeO$_2$ nanoparticles as radical scavengers adjacent (Sca$^{ad-CeO2}$) to Fe–N$_4$ sites (Fig. 7).[68] This configuration allowed radical formation at Fe–N$_4$ sites, reducing the lifespan as well as the impact of the radicals. This strategy helps to protect the active sites and enhance the durability of the Fe–N$_4$ catalysts.

3. Dynamic evolution of M–N–C catalysts

Generally, the dynamic evolution of the M–N$_x$ moiety in M–N–C catalysts is ubiquitous in electrocatalytic reactions.[69] In a suitable voltage range, electronic and structural catalytic centers may undergo reversible structural changes, in which the M–N–C structure can be restored upon removal of the applied voltage.[70] When the applied voltage exceeds the maximum value that the catalyst can withstand, the catalytic centers exhibit irreversible changes, such as carbon oxidation by radicals,
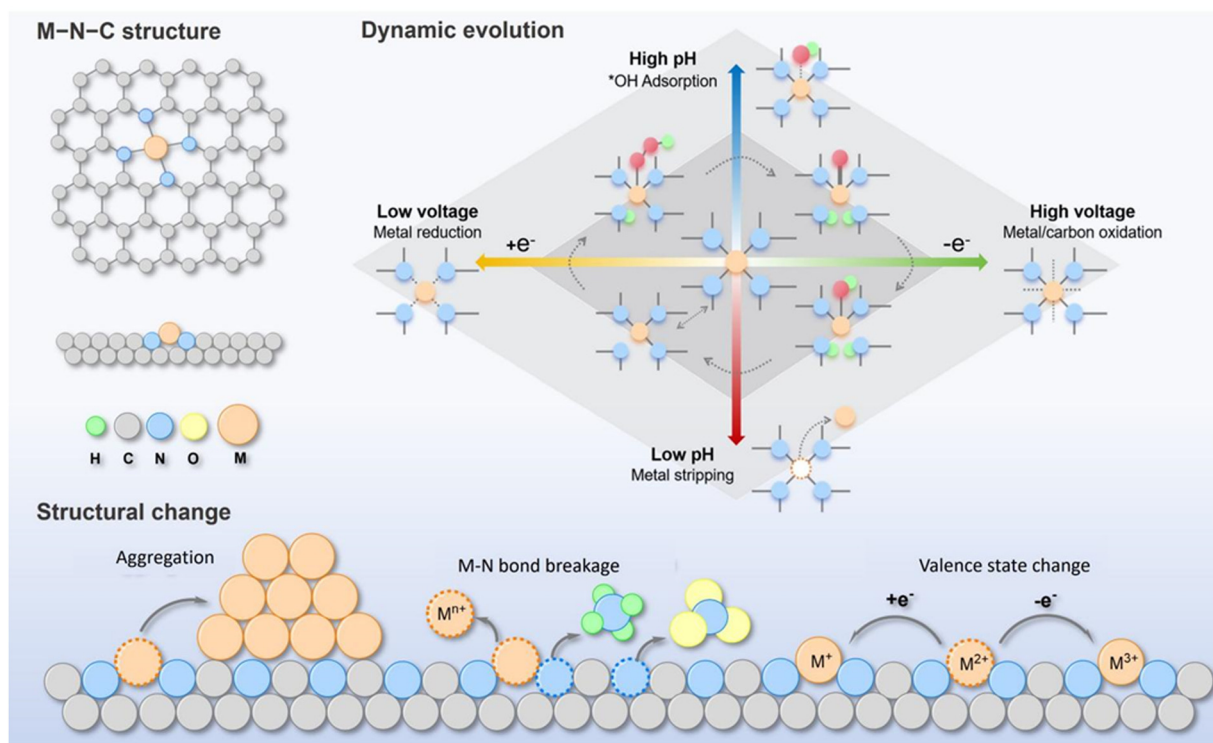
Fig. 8 Schematic illustration of voltage/pH-driven structural evolution of M–N–C catalysts.

oxidation and reduction of metal sites, and carbon corrosion (Fig. 8).[71] These changes show that the M–N–C structure evolves dynamically with changes in the reaction environment.[28] Therefore, the real active site in M–N–C under working conditions was substantially distinct from the as-synthesized M–N–C structure. This result indicated that the dynamic change was either beneficial or harmful depending on the specific case, thereby leading to the activation or degradation of the catalysts. Catalyst degradation indicates catalyst instability, thereby posing a serious challenge for industry implementation. Therefore, addressing the mechanism underlying the dynamic change is crucial to elucidate the reaction mechanism. In this section, examples of reversible and irreversible structural changes in M–N–C are summarized.

3.1. Reversible structural changes

In the electrochemical reactions catalyzed by M–N–C, both the applied voltage and the adsorption of reactants, intermediates, and products drive the dynamic evolution of the M–N_x moiety.[68] A stable catalyst is considered if the active sites are reconstructed under an applied voltage, and the structure is restored upon removal of the applied voltage. To date, the dynamic evolution of some common M–N–C electrocatalysts has been reported, and recent studies have focused on the structural variation of M–N–C configurations as well as the valence state variation of metal centers.[72,73] Fu et al. effectively constructed a Mn-SAS catalyst with uniform and precise Mn–N_4 configurations by pyrolyzing ZIF derivatives.[74] Although the initial structure did not change before and after the electrochemical ORR, as revealed through operando XAS, it experienced

structural dynamic evolution from the initial Mn–N_4 to Mn–N_3C and then to Mn–N_2C_2 during the intermediate reaction processes. Furthermore, the Mn metal centers underwent a series of valence state changes from +3.0 to +3.8 and then to +3.2. Wang et al. also confirmed that Cu–N–C remains oxidized and atomically dispersed after extended hours of electrocatalysis and revealed potential-driven restructuring of Cu–N–C to Cu nanoparticles through operando XAS in the electroreduction NO_3^-RR process (Fig. 9a and b).[59] The aggregated Cu nanoparticles were reversibly disintegrated into single atoms and then restored to the Cu–N_4 structure upon exposure to an oxidative ambient atmosphere for reversible structural changes (Fig. 9c). Cuenya et al. investigated the reversible structural evolution of various M–N–C catalysts (M = Fe, Sn, Cu, Co, Ni, Zn) in the CO_2RR through operando XAS.[75] Metallic clusters/nanoparticles were reversibly formed in most M–N–C catalysts during the CO_2RR process, except for Ni–N–C. Experiments have indicated that the competition between M–O and M–N interactions is an important factor in determining the mobility of metal species in M–N–C. Specifically, in comparison with other transition metals, the strong interaction between the Ni metal centers and the N-functional groups of the carbon support led to a higher stability of single Ni sites, leading to the excellent performance of Ni–N–C in the electrochemical CO_2-to-CO reaction.

3.2. Irreversible structural changes

In most cases, the stability of M–N–C catalysts is unsatisfactory, especially under harsh conditions involving extreme pH and applied potentials. The primary factors contributing to their instability include the oxidation of carbon, which supports the
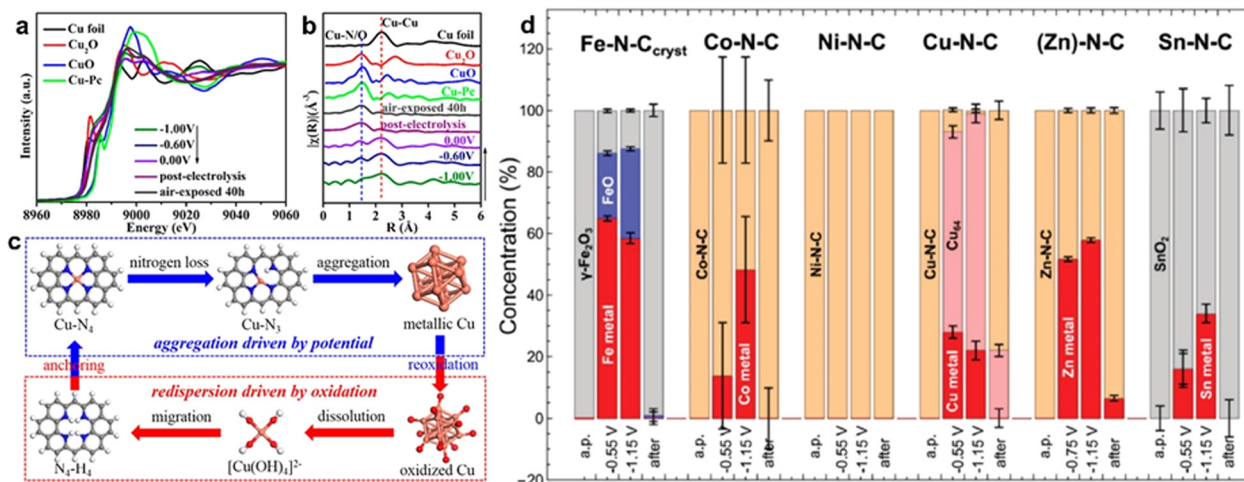
Fig. 9 (a) Cu K-edge XANES spectra at different potentials. (b) Cu K edge FT-EXAFS spectra by switching potentials (*vs.* RHE). (c) Proposed mechanisms of aggregation driven by the applied potential and redispersion.[59] Copyright 2022, Wiley-VCH. (d) Speciation of M–N–C catalysts in the as-prepared state, during CO_2RR at potentials (*vs.* RHE) indicated in the plot, and when exposed to air after CO_2RR.[75] Copyright 2024, Wiley-VCH.

demetallation of M–N_x active sites due to oxidation conditions, and the agglomeration of metal atoms under reduction conditions. The irreversible structural changes of various metal centers in M–N–C exhibit some similarities in terms of the types and drivers of structural evolution. M–N–C can change the electronic and coordination structure without changing the nucleus, or they can merge into clusters or nanoparticles under harsh activation and reaction conditions. These transformations are driven by external stimuli, adsorption–metal interactions, and carrier–metal interactions.[8] These structural changes are typically observable through various characterization techniques, and shifts in activity or selectivity can often be detected experimentally, thereby exhibiting different kinetic behaviors in their mediated reactions. Wei *et al.* reported the formation of a high-valence HO–Co–N_2 moiety due to the interaction between isolated Co–N_4 sites and electrolyte hydroxide, indicating that the highly oxidized Co sites were responsible for the catalytic performance under alkaline HER.[8] Liu *et al.* identified the structural evolution of M–N–C at the atomic level through cutting-edge *operando* XAS and SR-FTIR spectroscopy.[76] Single-atom Ni at solid–liquid interfaces tends to form $Ni_1^{(2-\delta)+}N_2$ during the ORR process, which plays a crucial role in the adsorption and dissociation of O_2 into *O intermediates. These results indicated that the thermodynamically stable M–N_4–C structure was destroyed under working conditions, thereby transforming into low-coordinated active sites.[70]

Under extreme conditions, the original anchoring sites of metal atoms are removed from the surface, shifting the individual metal atoms and eventually coalescing into aggregates of a few nanometers, thereby resulting in a change in activity/selectivity. This phenomenon is especially prevalent in continuous, high-current-density reactions, where M–N–C catalysts are prone to structural changes under sustained large-current operations. Our group investigated the structural evolution of M–N–C (M = Co, Ni, and Fe) catalysts in the OER and HER processes (Fig. 10).[77,78] In the OER process, the M–N–C

catalysts gradually aggregated to form MOOH nanoclusters with a carbon support as the active species for enhanced alkaline OER activity. N was first oxidized and dissolved in the form of NO_3^-, leaving various O functional groups on the carbon support and resulting in the destruction of the Ni–N bonds. Structural degradation also occurred in all three M–N–C catalysts during long-term HER in alkaline electrolytes at an industrial-grade current density. Both M–N and N–C bonds were gradually broken, thereby leading to initial performance decay and the release of M ions as well as NH_4^+ to the electrolyte. Additionally, newly formed metal-based nanoparticles were formed on the carbon substrate, thereby exhibiting different core–shell structures: Co@MWCNTs, Ni@Ni(OH)$_2$, and FeO@Fe(OH)$_3$.

4. Advanced characterization techniques

Understanding the dynamic evolution of M–N–C catalysts is crucial for elucidating the mechanisms behind catalyst degradation under operating conditions and for guiding strategies to increase stability. Therefore, advanced characterization techniques are very important for dynamically studying the entire change process of the M–N–C structure.[79,80] Additionally, owing to the occurrence of dynamic evolution, the structural features of the initial catalyst obtained *via ex situ* techniques are insufficient for describing the real active sites and structure–property relationships of M–N–C catalysts. Therefore, the development of *in situ*/*operando* characterization techniques for real-time monitoring of the dynamic evolution of M–N–C electrocatalysts and reaction intermediates has been achieved in recent decades, thereby bridging the understanding of fundamental mechanisms for the practical development of electrocatalysts. Given these functions, advanced characterization techniques can be classified into two categories: the characterization
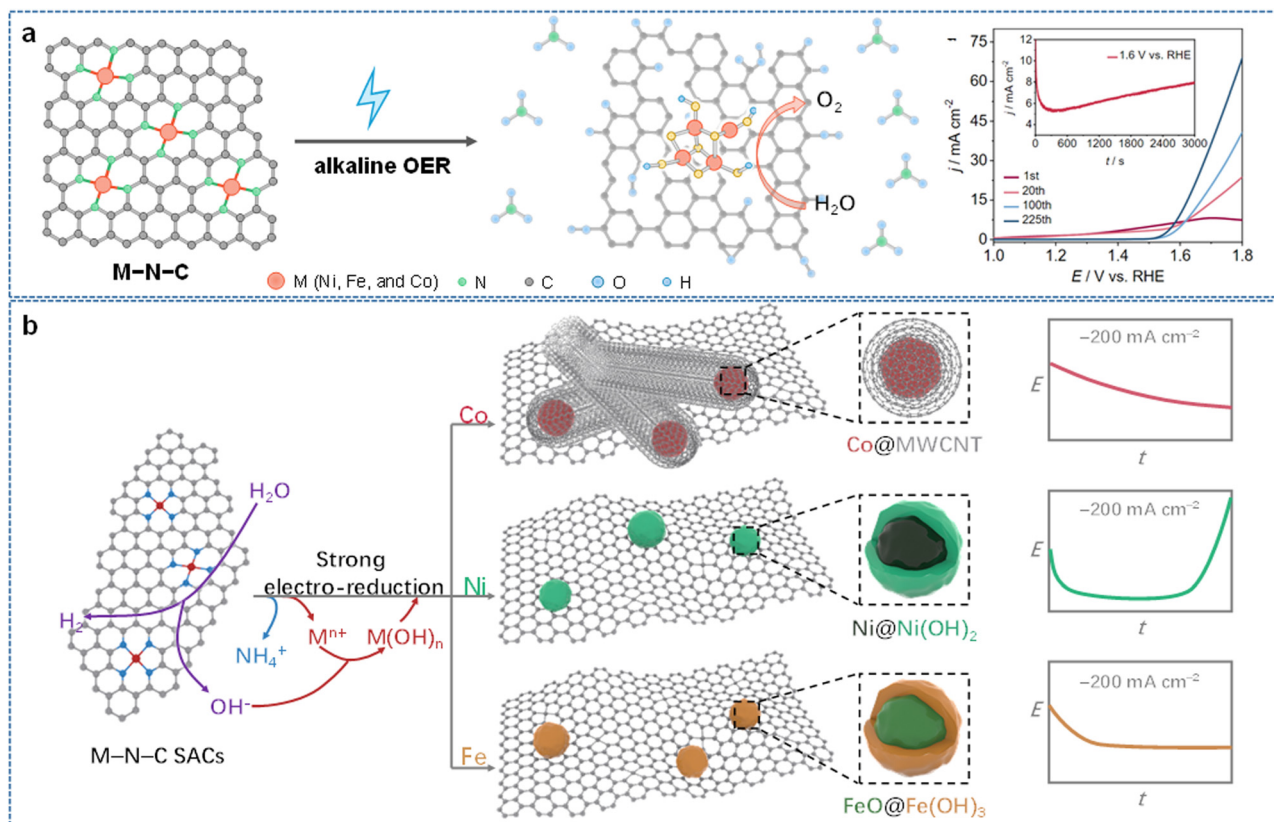
Fig. 10 (a) The mechanism of structural evolution of M−N−C (M = Co, Ni, and Fe) catalyst during the OER.[78] Copyright 2024, Wiley-VCH. (b) Illustration of the mechanism of structural degradation of M−N−C catalysts after long-term and industrial-grade current density HER.[77] Copyright 2024, Wiley-VCH.
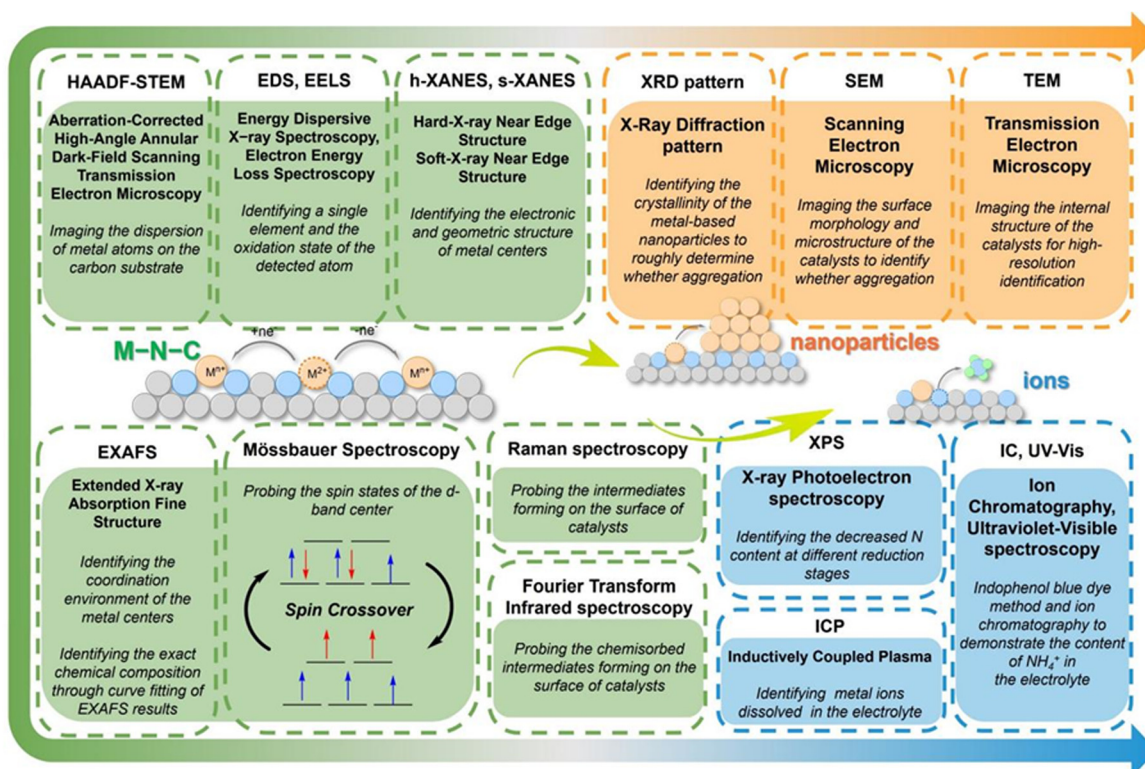

Fig. 11 Characterization methods.

of morphological changes and the characterization of coordination or electronic structural changes (Fig. 11).

For the morphological structure, high-resolution electron microscopy techniques, including scanning electron microscopy (SEM), transmission electron microscopy (TEM), high-angle annular dark-field STEM (HAADF-STEM), and scanning tunneling microscopy, were employed to resolve the morphological structure changes before and after the electrocatalytic reactions. In particular, HAADF-STEM, a frequently used technique for distinguishing heavy atoms, offers intuitive evidence for detecting the metal atom distribution of M–N–C due to the contrast in the atomic number contrast between the active metal atoms and their carbon supports. Zhang et al. utilized subångström-resolution aberration-corrected HAADF-STEM to identify the atomic dispersion of Fe in three Fe–N–C catalysts.[81] This technique distinguishes single Fe atoms from small particles measuring 3–5 nm in size. Additionally, energy dispersive X-ray spectroscopy (EDS) and electron energy loss spectroscopy (EELS) were used to identify individual elements and determine the oxidation states of the atoms. These techniques are particularly effective when metal atoms are embedded on the surface of a two-dimensional material carrier or localized within an internal region of the carrier, thereby offering detailed information about the oxidation states of the metal atoms.[82] Wu et al. employed aberration-corrected STEM imaging coupled with EELS to investigate the atomic dispersion and local environment of Mn at an atomic resolution.[36] A point EEL spectrum was obtained by positioning a 1 Å electron probe directly on a single Mn atom. The signal from the EEL point spectrum originates from the atom and its closest neighboring atoms. The coexistence of N and a single Mn atom within this ångström-scale region strongly indicated an Mn–N coordination structure, thereby offering compelling evidence of the immediate vicinity of Mn and N in a coordinated framework.

For coordination/electronic structures, synchrotron-based techniques are employed to identify the electronic structure and coordination configuration of M–N–C catalysts. Specifically, XAS plays an important role in identifying the environment of the metal centers, thereby offering vital information.[83,84] Additionally, X-ray absorption near-edge structure (XANES) spectra, with energies ranging from the absorption edge of 30 eV to 50 eV, offer detailed information about the oxidation state, symmetry, and coordination ligand environment of M–N–C. It is very sensitive to the electronic environment, oxidation state, and local symmetry of the element. Hard-X-ray near-edge structure (h-XANES) and soft-X-ray near-edge structure (s-XANES) methods are often used to identify the electronic and geometric structures of metals and their surrounding atoms (C, N, and O).[85] Furthermore, extended X-ray absorption fine structure (EXAFS), in which the energy ranges from the absorption edge of 50 eV to 1000 eV or more, offers detailed structural and coordination information, such as the number of different coordinating species and their distances from the absorber atom, the angles between chemical bonds, and the degree of thermal disorder.[86] Hu et al. employed operando XAS and fitting data to reveal that Co–N–C underwent significant structural changes upon immersion in an alkaline electrolyte.

These changes were followed by Fe incorporation during electrochemical activation, thereby resulting in the formation of a dimeric Co–Fe structural motif.[87] For specific metal centers, such as Fe, Sn, Au, Ru, and Ir, Mössbauer spectroscopy can probe the spin states of the d-band center.[56]

In addition to these techniques, several effective characterization techniques have been used under special conditions. For example, operando synchrotron Fourier transform infrared spectroscopy (SR-FTIR) combined with operando XAS can reveal the atomic-level dynamics of active site evolution at solid–liquid electrochemical interfaces, thereby tracking the reactive intermediates on M–N–C catalysts during the electrochemical process.[76,84,88] Diffusion reflectance infrared Fourier transform spectroscopy (DRIFTS) is employed to examine the adsorption behaviors of probe molecules such as CO and NO, differentiating between single-atom M–N–C structures and clusters or nanoparticles.[89,90] Flytzani-Stephanopoulos et al. utilized IR spectroscopy to identify isolated Pt atoms by analysing the binding strength of CO molecules and metal atoms.[89] Operando Raman spectroscopy can provide insights into structural fingerprints and metal–substrate interactions in carbon substrates.[91] Notably, combining multiple operando methods can offer a comprehensive understanding of dynamic structural evolution.

5. Conclusion and outlook

Over the past decade, M–N–C catalysts have significantly advanced in the field of electrocatalysis because of their distinct geometry and electrical structures, thereby positioning them as potential replacements for precious metal-based catalysts. The dynamic evolution of M–N–C catalysts during electrochemical reactions has garnered increasing attention. This review summarizes the factors affecting the stability of M–N–C catalysts in electrocatalytic reactions. The inherent factors include metallic centers and coordination configurations, as well as external factors such as pH, applied voltage, and reaction intermediates. Strategies to increase the stability of M–N–C catalysts, such as designing bimetal centers through electronic regulation and employing free radical quenchants, are discussed. Furthermore, reversible structural changes in M–N–C catalysts were reviewed, especially in the ORR and CO_2RR processes. Notably, under certain extreme conditions, these M–N–C catalysts can undergo irreversible changes. Advanced characterization techniques are crucial for efficiently elucidating the dynamic revolution of M–N–C catalysts, thereby predicating their working mechanisms and identifying the real active centers in electrocatalysis.

Despite this progress, further development is needed in the following areas to advance our understanding and practical application of M–N–C catalysts. (i) Identification of real active sites in M–N–C catalysts during the electrocatalytic reaction is important. Furthermore, combining advanced operando techniques with theoretical calculations, such as DFT or finite element analysis, offers a powerful approach for understanding dynamic structural evolution and revealing real active sites.

The integration of these methods is expected to provide a clear roadmap of how catalyst active sites evolve during reactions and their correlation with performance as well as reaction mechanisms. (ii) Enhancing the long-term electrochemical durability of M–N–C catalysts is essential. Currently, M–N–C catalysts with atomically dispersed metal atoms fall short compared with commercial precious metal-based catalysts, especially under harsh electrochemical reaction conditions. Stability tests for M–N–C electrocatalysts have shown lifespans ranging from 1 h to 100 h in preliminary laboratory tests, which is insufficient for industrial applications. Thus, methods to increase the electrochemical stability of real active sites in M–N–C catalysts are urgently needed. Finally, a combination of advanced *operando* techniques and theoretical calculations will be vital in unravelling the mechanistic origins of M–N–C catalysts and guiding their designs, thereby increasing their stability. The development of advanced characterization techniques, theoretical calculations, and stability enhancement strategies will not only provide accurate insights into the activity of M–N–C catalysts but also facilitate the selection of stable candidates for effective electrocatalytic reactions.

Data availability

No primary research results, software or code have been included and no new data were generated or analysed as part of this review.

Conflicts of interest

There are no conflicts to declare.

Acknowledgements

Notes and references

1 M. Shao, Q. Chang, J.-P. Dodelet and R. Chenitz, *Chem. Rev.*, 2016, **116**, 3594–3657.
2 Z. Zhang, S. Li, Z. Zhang, Z. Chen, H. Wang, X. Meng, X. Cui, X. Qi and J. Wang, *Carbon Energy*, 2024, **6**, e531.
3 H. Sun, Z. Yan, F. Liu, W. Xu, F. Cheng and J. Chen, *Adv. Mater.*, 2020, **32**, 1806326.
4 X. Xu, H. Sun, S. Jiang and Z. Shao, *SusMat*, 2021, **1**, 460–481.
5 X. Zhang, Y. Wang, Y. Wang, Y. Guo, X. Xie, Y. Yu and B. Zhang, *Chem. Commun.*, 2022, **58**, 2777–2787.
6 Y. Wang, C. Wang, M. Li, Y. Yu and B. Zhang, *Chem. Soc. Rev.*, 2021, **50**, 6720–6733.
7 Y. Jiao, Y. Zheng, M. Jaroniec and S. Z. Qiao, *Chem. Soc. Rev.*, 2015, **44**, 2060–2086.
8 L. Cao, Q. Luo, W. Liu, Y. Lin, X. Liu, Y. Cao, W. Zhang, Y. Wu, J. Yang, T. Yao and S. Wei, *Nat. Catal.*, 2019, **2**, 134–141.
9 B. Qiao, A. Wang, X. Yang, L. F. Allard, Z. Jiang, Y. Cui, J. Liu, J. Li and T. Zhang, *Nat. Chem.*, 2011, **3**, 634–641.
10 Y. Wang, H. Su, Y. He, L. Li, S. Zhu, H. Shen, P. Xie, X. Fu, G. Zhou, C. Feng, D. Zhao, F. Xiao, X. Zhu, Y. Zeng, M. Shao, S. Chen, G. Wu, J. Zeng and C. Wang, *Chem. Rev.*, 2020, **120**, 12217–12314.
11 C. Zhu, S. Fu, Q. Shi, D. Du and Y. Lin, *Angew. Chem., Int. Ed.*, 2017, **56**, 13944–13960.
12 H. Liu, J. Li, J. Arbiol, B. Yang and P. Tang, *EcoEnergy*, 2023, **1**, 154–185.
13 C. Gao, J. Low, R. Long, T. Kong, J. Zhu and Y. Xiong, *Chem. Rev.*, 2020, **120**, 12175–12216.
14 W. Zhang, W. Lai and R. Cao, *Chem. Rev.*, 2017, **117**, 3717–3797.
15 S. K. Kaiser, Z. Chen, D. Faust Akl, S. Mitchell and J. Pérez-Ramírez, *Chem. Rev.*, 2020, **120**, 11703–11809.
16 M.-K. Wong, J. J. Foo, J. Y. Loh and W.-J. Ong, *Adv. Energy Mater.*, 2024, **14**, 2303281.
17 H. Su, S. Song, N. Li, Y. Gao, P. Li, L. Ge and T. Ma, *Adv. Energy Mater.*, 2023, **13**, 2301547.
18 Z. Qi, Y. Zhou, R. Guan, Y. Fu and J.-B. Baek, *Adv. Mater.*, 2023, **35**, 2210575.
19 S. Wei, R. Yang, Z. Wang, J. Zhang and X.-H. Bu, *Adv. Mater.*, 2024, **15**, 5082.
20 F. Liu, Y. Guo, Y. Zhong, J. Li, H. Zhang, L. Shi, X. Lin, F. Ye, K. Ge, S. Yuan, C. Hu and C. Guo, *Chem. Commun.*, 2024, **60**, 4064–4067.
21 L. Zhang, Q. Meng, R. Zheng, L. Wang, W. Xing, W. Cai and M. Xiao, *Nano Res.*, 2023, **16**(4), 4468–4487.
22 J. Fonseca and J. Lu, *ACS Catal.*, 2021, **11**, 7018–7059.
23 L. Wang, H. Wang and J. Lu, *Chem. Catal.*, 2023, **3**, 100492.
24 W. Ma, Z. Deng, X. J. Zhang, Z. Zhang and Z. Zhou, *J. Mater. Chem. A*, 2023, **11**, 12643–12658.
25 P. Rao, D. Wu, T.-J. Wang, J. Li, P. Deng, Q. Chen, Y. Shen, Y. Chen and X. Tian, *eScience*, 2022, **2**, 399–404.
26 G. Di Liberto, L. Giordano and G. Pacchioni, *ACS Catal.*, 2024, **14**, 45–55.
27 L. Liu, T. Chen and Z. Chen, *Adv. Sci.*, 2024, **11**, 2308046.
28 X. Li, C.-S. Cao, S.-F. Hung, Y.-R. Lu, W. Cai, A. I. Rykov, S. Miao, S. Xi, H. Yang, Z. Hu, J. Wang, J. Zhao, E. E. Alp, W. Xu, T.-S. Chan, H. Chen, Q. Xiong, H. Xiao, Y. Huang, J. Li, T. Zhang and B. Liu, *Chem*, 2020, **6**, 3440–3454.
29 L. Zhang, J. Yang, X. Yang, A. Wang and T. Zhang, *Chem. Catal.*, 2023, **3**, 100560.
30 H. Hu, J. Wang, P. Tao, C. Song, W. Shang, T. Deng and J. Wu, *J. Mater. Chem. A*, 2022, **10**, 5835–5849.
31 X. Xu, Y. Zhong, M. Wajrak, T. Bhatelia, S. Jiang and Z. Shao, *InfoMat*, 2024, **6**, e12608.
32 G. A. Lawrance, *Introduction to Coordination Chemistry*, John Wiley & Sons Ltd, 2010, 56–57.
33 Y. Ren, J. Wang, M. Zhang, Y. Wang, Y. Cao, D. H. Kim, Y. Liu and Z. Lin, *Small*, 2024, **20**, 2308213.
34 W. C. Lai, Z. S. Ma, J. W. Zhang, Y. L. Yuan, Y. Qiao and H. W. Huang, *Adv. Funct. Mater.*, 2022, **32**, 2111193.
35 C. Zheng, X. Zhang, Z. Zhou and Z. Hu, *eScience*, 2022, **2**, 219–226.
36 J. Li, M. Chen, D. A. Cullen, S. Hwang, M. Wang, B. Li, K. Liu, S. Karakalos, M. Lucero, H. Zhang, C. Lei, H. Xu, G. E. Sterbinsky, Z. Feng, D. Su, K. L. More, G. Wang, Z. Wang and G. Wu, *Nat. Catal.*, 2018, **1**, 935–945.
37 Y. Zhong, X. Liang, Z. He, W. Tan, J. Zhu, P. Yuan, R. Zhu and H. He, *Appl. Catal., B*, 2014, **150–151**, 612–618.
38 Y. Gao, B. Liu and D. Wang, *Adv. Mater.*, 2023, **35**, 2209654.
39 Q. Jia, N. Ramaswamy, H. Hafiz, U. Tylus, K. Strickland, G. Wu, B. Barbiellini, A. Bansil, E. F. Holby, P. Zelenay and S. Mukerjee, *ACS Nano*, 2015, **9**, 12496–12505.
40 Z. Miao, X. Wang, Z. Zhao, W. Zuo, S. Chen, Z. Li, Y. He, J. Liang, F. Ma, H.-L. Wang, G. Lu, Y. Huang, G. Wu and Q. Li, *Adv. Mater.*, 2021, **33**, 2006613.
41 J. Wang, W. Qiu, G. Li, J. Liu, D. Luo, Y. Zhang, Y. Zhao, G. Zhou, L. Shui, X. Wang and Z. Chen, *Energy Storage Mater.*, 2022, **46**, 269–277.
42 H. H. Wong, M. Sun, T. Wu, C. H. Chan, L. Lu, Q. Lu, B. Chen and B. Huang, *eScience*, 2024, **4**, 100140.
43 T. Patniboon and H. A. Hansen, *ACS Catal.*, 2021, **11**, 13102–13118.
44 J. Liu, X. Wan, S. Liu, X. Liu, L. Zheng, R. Yu and J. Shui, *Adv. Mater.*, 2021, **33**, 2103600.
45 H. Shang, W. Sun, R. Sui, J. Pei, L. Zheng, J. Dong, Z. Jiang, D. Zhou, Z. Zhuang, W. Chen, J. Zhang, D. Wang and Y. Li, *Nano Lett.*, 2020, **20**, 5443–5450.
46 J. Li, M. T. Sougrati, A. Zitolo, J. M. Ablett, I. C. Oğuz, T. Mineva, I. Matanovic, P. Atanassov, Y. Huang, I. Zenyuk, A. Di Cicco, K. Kumar, L. Dubau, F. Maillard, G. Dražić and F. Jaouen, *Nat. Catal.*, 2021, **4**, 10–19.
47 Z. Wang, X. Jin, R. Xu, Z. Yang, S. Ma, T. Yan, C. Zhu, J. Fang, Y. Liu, S.-J. Hwang, Z. Pan and H. J. Fan, *ACS Nano*, 2023, **17**, 8622–8633.

48 Y. Ying, X. Luo, J. Qiao and H. Huang, *Adv. Funct. Mater.*, 2021, **31**, 2007423.

49 X. Cheng, J. Yang, W. Yan, Y. Han, X. Qu, S. Yin, C. Chen, R. Ji, Y. Li, G. Li, G. Li, Y. Jiang and S. Sun, *Energy Environ. Sci.*, 2021, **14**, 5958–5967.

50 M. Dan, X. Zhang, Y. Yang, J. Yang, F. Wu, S. Zhao and Z.-Q. Liu, *Proc. Natl. Acad. Sci. U. S. A.*, 2024, **121**, e2318174121.

51 C. Hu, G. Xing, W. Han, Y. Hao, C. Zhang, Y. Zhang, C.-H. Kuo, H.-Y. Chen, F. Hu, L. Li and S. Peng, *Adv. Mater.*, 2024, **26**, 2405763.

52 N. Karmodak and J. K. Nørskov, *Angew. Chem., Int. Ed.*, 2023, **62**, e202311113.

53 D. Zhang, Z. Wang, F. Liu, P. Yi, L. Peng, Y. Chen, L. Wei and H. Li, *J. Am. Chem. Soc.*, 2024, **146**, 3210–3219.

54 J. Cai, X. Hao, Z. Bian, Y. Wu, C. Wei, X. Yin, B. Liu, M. Fang, Y. Lv, Y. Xie, Y. Fang and G. Wang, *Angew. Chem., Int. Ed.*, 2024, **63**, e202409079.

55 P. G. Santori, F. D. Speck, J. Li, A. Zitolo, Q. Jia, S. Mukerjee, S. Cherevko and F. Jaouen, *J. Electrochem. Soc.*, 2019, **166**, F3311–F3320.

56 N. R. Sahraie, U. I. Kramm, J. Steinberg, Y. Zhang, A. Thomas, T. Reier, J.-P. Paraknowitsch and P. Strasser, *Nat. Commun.*, 2015, **6**, 8618.

57 H. Zhong, Q. Zhang, J. Yu, X. Zhang, C. Wu, Y. Ma, H. An, H. Wang, J. Zhang, X. Wang and J. Xue, *Adv. Energy Mater.*, 2023, **13**, 2301391.

58 H. Zhang, Y. Liu, T. Chen, J. Zhang, J. Zhang and X. W. Lou, *Adv. Mater.*, 2019, **31**, 1904548.

59 J. Yang, H. Qi, A. Li, X. Liu, X. Yang, S. Zhang, Q. Zhao, Q. Jiang, Y. Su, L. Zhang, J.-F. Li, Z.-Q. Tian, W. Liu, A. Wang and T. Zhang, *J. Am. Chem. Soc.*, 2022, **144**, 12062–12071.

60 X. Hu, S. Chen, L. Chen, Y. Tian, S. Yao, Z. Lu, X. Zhang and Z. Zhou, *J. Am. Chem. Soc.*, 2022, **144**, 18144–18152.

61 E. F. Holby, G. Wang and P. Zelenay, *ACS Catal.*, 2020, **10**, 14527–14539.

62 F. D. Speck, A. Zagalskaya, V. Alexandrov and S. Cherevko, *Angew. Chem., Int. Ed.*, 2021, **60**, 13343–13349.

63 A. Kormányos, F. D. Speck, K. J. J. Mayrhofer and S. Cherevko, *ACS Catal.*, 2020, **10**, 10858–10870.

64 P. Hutchison, P. S. Rice, R. E. Warburton, S. Raugei and S. Hammes-Schiffer, *J. Am. Chem. Soc.*, 2022, **144**(36), 16524–16534.

65 A. S. Dobrota, N. V. Skorodumova, S. V. Mentus and I. A. Pašti, *Electrochim. Acta*, 2022, **412**, 140155.

66 X. Tan, H. A. Tahini and S. C. Smith, *J. Mater. Chem. A*, 2021, **9**, 8721–8729.

67 C. H. Choi, H.-K. Lim, M. W. Chung, G. Chon, N. Ranjbar Sahraie, A. Altin, M.-T. Sougrati, L. Stievano, H. S. Oh, E. S. Park, F. Luo, P. Strasser, G. Dražić, K. J. J. Mayrhofer, H. Kim and F. Jaouen, *Energy Environ. Sci.*, 2018, **11**, 3176–3182.

68 X. Cheng, X. Jiang, S. Yin, L. Ji, Y. Yan, G. Li, R. Huang, C. Wang, H. Liao, Y. Jiang and S. Sun, *Angew. Chem., Int. Ed.*, 2023, **62**, e202306166.

69 Y. Zhang, H. Liu, S. Zhao, C. Xie, Z. Huang and S. Wang, *Adv. Mater.*, 2023, **35**, 2209680.

70 J. Yang, W. Liu, M. Xu, X. Liu, H. Qi, L. Zhang, X. Yang, S. Niu, D. Zhou, Y. Liu, Y. Su, J.-F. Li, Z.-Q. Tian, W. Zhou, A. Wang and T. Zhang, *J. Am. Chem. Soc.*, 2021, **143**, 14530–14539.

71 S. Lu, C. Cheng, Y. Shi, Y. Wu, Z. Zhang and B. Zhang, *Proc. Natl. Acad. Sci. U. S. A.*, 2023, **120**, e2300549120.

72 X. Bai, X. Zhao, Y. Zhang, C. Ling, Y. Zhou, J. Wang and Y. Liu, *J. Am. Chem. Soc.*, 2022, **144**, 17140–17148.

73 D. Karapinar, N. T. Huan, N. R. Sahraie, J. Li, D. Wakerley, N. Touati, S. Zanna, D. Taverna, L. H. G. Tizei, A. Zitolo, F. Jaouen, V. Mougel and M. Fontecave, *Angew. Chem., Int. Ed.*, 2019, **58**, 15098–15103.

74 M. Tong, F. Sun, G. Xing, C. Tian, L. Wang and H. Fu, *Angew. Chem., Int. Ed.*, 2023, **62**, e202314933.

75 D. Hursán, J. Timoshenko, E. Ortega, H. S. Jeon, M. Rüscher, A. Herzog, C. Rettenmaier, S. W. Chee, A. Martini, D. Koshy and B. Roldán Cuenya, *Adv. Mater.*, 2024, **36**, 2307809.

76 H. Su, W. Zhou, H. Zhang, W. Zhou, X. Zhao, Y. Li, M. Liu, W. Cheng and Q. Liu, *J. Am. Chem. Soc.*, 2020, **142**, 12306–12313.

77 Q. Ruan, S. Lu, J. Wu, Y. Shi and B. Zhang, *Angew. Chem., Int. Ed.*, 2024, **63**, e202409000.

78 S. Lu, Z. Zhang, C. Cheng, B. Zhang and Y. Shi, *Angew. Chem., Int. Ed.*, 2024, **62**, e202413308.

79 X. Li, X. Yang, J. Zhang, Y. Huang and B. Liu, *ACS Catal.*, 2019, **9**, 2521–2531.

80 C. Liu, Y. Cui and Y. Zhou, *Energy Mater.*, 2025, **5**, 500001.

81 W. Liu, L. Zhang, X. Liu, X. Liu, X. Yang, S. Miao, W. Wang, A. Wang and T. Zhang, *J. Am. Chem. Soc.*, 2017, **139**, 10790–10798.

82 M. Lopez-Haro, L. Dubau, L. Guetaz, P. Bayle-Guillemaud, M. Chatenet, J. Andre, N. Caque, E. Rossinot and F. Maillard, *Appl. Catal., B*, 2014, **152**, 300–308.

83 Y. Zhu, T.-R. Kuo, Y.-H. Li, M.-Y. Qi, G. Chen, J. Wang, Y.-J. Xu and H. M. Chen, *Energy Environ. Sci.*, 2021, **14**, 1928–1958.

84 B. B. Sarma, F. Maurer, D. E. Doronkin and J.-D. Grunwaldt, *Chem. Rev.*, 2023, **123**, 379–444.

85 A. Zitolo, N. Ranjbar-Sahraie, T. Mineva, J. Li, Q. Jia, S. Stamatin, G. F. Harrington, S. M. Lyth, P. Krtil, S. Mukerjee, E. Fonda and F. Jaouen, *Nat. Commun.*, 2017, **8**, 957.

86 L. Cao, W. Liu, Q. Luo, R. Yin, B. Wang, J. Weissenrieder, M. Soldemo, H. Yan, Y. Lin, Z. Sun, C. Ma, W. Zhang, S. Chen, H. Wang, Q. Guan, T. Yao, S. Wei, J. Yang and J. Lu, *Nature*, 2019, **565**, 631–635.

87 L. Bai, C. Hsu, D. T. L. Alexander, H. Chen and X. Hu, *J. Am. Chem. Soc.*, 2019, **141**(36), 14190–14199.

88 J.-Y. Ye, Y.-X. Jiang, T. Sheng and S.-G. Sun, *Nano Energy*, 2016, **29**, 414–427.

89 J. Liu, F. R. Lucci, M. Yang, S. Lee, M. D. Marcinkowski, A. J. Therrien, C. T. Williams, E. C. H. Sykes and M. Flytzani-Stephanopoulos, *J. Am. Chem. Soc.*, 2016, **138**, 6396–6399.

90 J. Zhou, S. Han, R. Yang, T. Li, W. Li, Y. Wang, Y. Yu and B. Zhang, *Angew. Chem., Int. Ed.*, 2023, **62**, e202305184.

91 Y. Zhao, T. Ling, S. Chen, B. Jin, A. Vasileff, Y. Jiao, L. Song, J. Luo and S.-Z. Qiao, *Angew. Chem., Int. Ed.*, 2019, **58**, 12252–12257.